PCCP

PAPER

Cite this: *Phys. Chem. Chem. Phys.*, 2015, **17**, 12804

Genericity of confined chemical garden patterns with regard to changes in the reactants

Florence Haudin,[a] V. Brasiliense,[a] Julyan H. E. Cartwright,[b] Fabian Brau[a] and A. De Wit*[a]

Received 6th January 2015,
Accepted 14th April 2015

DOI: 10.1039/c5cp00068h

www.rsc.org/pccp

The growth of chemical gardens is studied experimentally in a horizontal confined geometry when a solution of metallic salt is injected into an alkaline solution at a fixed flow rate. Various precipitate patterns are observed—spirals, flowers, worms or filaments—depending on the reactant concentrations. In order to determine the relative importance of the chemical nature of the reactants and physical processes in the pattern selection, we compare the structures obtained by performing the same experiment using different pairs of reactants of varying concentrations with cations of calcium, cobalt, copper, and nickel, and anions of silicate and carbonate. We show that although the transition zones between different patterns are not sharply defined, the morphological phase diagrams are similar in the various cases. We deduce that the nature of the chemical reactants is not a key factor for the pattern selection in the confined chemical gardens studied here and that the observed morphologies are generic patterns for precipitates possessing a given level of cohesiveness when grown under certain flow conditions.

1 Introduction

Chemical gardens are self-assembled structures resulting from a precipitation reaction involving a metallic salt and an aqueous alkaline solution like, for example, silicate. They are typically grown in 3D and their basic mechanism of formation is qualitatively fairly well understood.[1–3] A solid seed of metallic salt is first immersed in an alkaline solution. A semipermeable membrane of metal silicate develops around the seed as the salt dissolves in the solution. Water from the solution is then pumped inside this membrane because of the osmotic pressure difference, leading to further dissolution of the salt. The membrane inflates until the stress exceeds the mechanical resistance of the membrane, which breaks and releases a generally less dense metal-rich solution into the alkaline outer solution, giving rise to further precipitation around the rising buoyant jet. This process leads, within seconds to hours, to the formation of irregular tubular structures resembling biological forms. These tubes may grow to lengths over a hundred times their initial diameter and tend to taper in diameter eventually to close to a point.[1,2]

Chemical gardens are currently the subject of intensive research. Understanding the mechanism of formation of the variety of spatial structures possible in chemical gardens remains indeed a challenge at the crossroad of disciplines as diverse and complementary as physics, chemistry, nonlinear pattern formation and materials science. It is of interest to understand their rich chemical, magnetic and electrical properties related to the steep pH and electrochemical gradients existing across their walls.[4,5] They also share common properties with structures as varied as corrosion filaments,[6] cement nanotubes,[7] brinicles[8] and chimneys at hydrothermal vents.[9] They are model systems to understand properties of self-organized materials[10–18] and fuel cells[19] and to study possible mechanisms for the origin of life.[20,21]

A large variety of water-soluble metallic salts can display growths of similar tubular structures. However, the rate of growth, the size and the shape of the excrescences may vary significantly depending on the precipitating cation of the metallic salt and the concentration and the chemical composition of the alkaline solution.[1] In concentrated solutions of silicate, a strong and dense membrane is formed around the dissolving salt, which ruptures only with difficulty to produce secondary growths leading to the formation of few wide tubes.[22] As the solution is made more dilute, the membrane becomes more "elastic" allowing the formation of clusters of narrow tubes by repeated rupture and rehealing of the colloidal envelope. With salts characterized by the same metal cation but different non-precipitating anionic species, the 3D pattern obtained is rather similar in each case; only differences in the growth rate are noticeable, perhaps due to variations in the solubility of the seed crystals in water.[1] For a given alkaline solution, the nature of the precipitating metal cation has been found to be a factor influencing the shape and the growth rate of the tubular structures. For example, calcium yields wider tubes with flexible thin walls whereas nickel produces

[a] *Nonlinear Physical Chemistry Unit, Faculté des Sciences, Université libre de Bruxelles (ULB), CP231, 1050 Brussels, Belgium. E-mail: adewit@ulb.ac.be*
[b] *Instituto Andaluz de Ciencias de la Tierra, CSIC-Universidad de Granada, Campus Fuentenueva, E-18071 Granada, Spain*

very robust tubes with thick walls; the tubular structures grown with manganese and cobalt have intermediate behaviors.[22] Strontium and barium produce short, narrow tubes that sometimes grow as clusters.[23] Copper and iron yield a dense cluster of much finer fibres compared to cobalt.[1,24] In all cases, there is a difference of composition between the inner and the outer part of the tubes; oxides and hydroxides inside and silicon compounds outside.[22]

One hindrance to quantitative studies of these tubular structures in classical chemical gardens is the erratic nature of the tube growth. Their formation mechanism implies the coupling between buoyancy, osmosis and reaction–diffusion processes, which in 3D complicates significantly the understanding of the system. To obtain more regular tubes, an aqueous metal-salt solution can be injected at a given flow rate through a capillary into the alkaline solution contained in a 3D beaker. Depending on the concentration of the injected solution, different growth regimes, such as popping, jetting, budding and ocean-ridge-like dynamics, have been observed.[25–27] Injection reduces the role played by osmosis during the growth and leads to the formation of regular tubes provided the concentration of metallic salt is not too large. Beyond some limit, wide bulging tubes are formed.[25] Buoyant gas bubbles can also be used to stabilize the tubular growth and select the tube radius.[28]

In order to have more control over the emerging patterns and to gain insight into their growth properties, chemical gardens have recently been grown by injection of solutions in a horizontal Hele-Shaw cell to confine the dynamics to a quasi-2D geometry and to reduce the influence of buoyancy and osmosis.[29] A Hele-Shaw cell consists of two parallel plates separated by a small interstice, see Fig. 1. In our case, this gap is filled with one of the solutions, and the other solution is injected radially at a constant flow rate, the reaction taking place in the contact zone between the two solutions.[29–32] Under such conditions, a large variety of reproducible precipitation patterns emerges. Fig. 2A shows a phase diagram obtained when cobalt chloride, $CoCl_2$, is injected into sodium silicate.[29] The various morphologies depend on the concentrations of both solutions and on the flow rate.

The physical and chemical mechanisms controlling the pattern selection of these quasi-2D chemical gardens are still essentially unknown, except for the spiral patterns for which the growth mechanism has been analysed.[29] As mentioned above, the nature of the precipitating metal ion of the salt is an important factor influencing the tubular growth in classical chemical gardens grown in 3D when a crystal seed dissolves in a silicate solution. Our objective is here to verify to what extent this remains true, and to investigate the importance of the precipitating anion from the displaced solution, for chemical gardens growing in a confined geometry. To do so, we study experimentally precipitation patterns obtained by injection of a metallic salt solution into an alkaline one in a Hele-Shaw cell for various recipes known to produce chemical gardens in 3D. We build morphological phase diagrams[24] for different pairs of reactants by varying the concentrations of both reactants at a fixed flow rate. We analyse the similarities and differences between the emerging structures and those of the phase diagram displayed in Fig. 2A, considered as a reference. We find that neither changes in the nature of the cation of the metallic salt solution or its pH, nor changes of the anion of the alkaline solution, influence significantly the precipitation patterns.

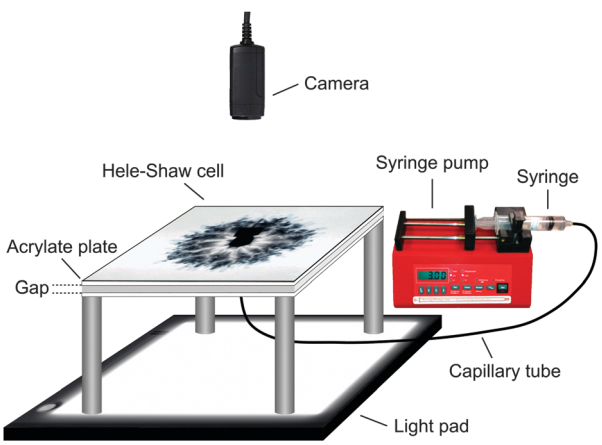

Fig. 1 Schematic diagram of the experimental setup described in Section 6.

2 Confined chemical garden patterns

Let us first recall and define the typical precipitation patterns obtained in flow conditions in confined Hele-Shaw cells. A representative selection of these structures is shown in Fig. 3A–D. The typical time evolution of similar patterns is shown in Fig. 3E–H. We observe the following structures. (i) Worms are fingers with slightly curved or undulating walls that sometimes exhibit some terrace structures. They are produced by the addition of new precipitates at the end of a given already formed worm (Fig. 3E). (ii) Spirals are growing buds delimited by spiraled walls; Fig. 3B shows a zoom in on a pair of them. Their growth is initiated from a point source with an initial radius growing up to rupture together with a rotation of the precipitate layer as a whole.[29] We can see in Fig. 3F the repetition of the process along the dashed lines. (iii) Flowers are patterns growing radially with an undulated contour where the precipitate is mainly located, forming ''petals'' (Fig. 3G). (iv) Filaments of type F1 are narrow 1D-like tubular structures. Their growth, the fastest among the patterns observed here (see Fig. 3H for F1 filaments), is the result of the addition of small segments, more or less tortuous, at the end of already formed filaments. Their growth is quite similar to that of the worms but at a smaller scale and with a faster growth rate. Two other structures can also sometimes emerge together with these F1 filaments (see Fig. 3D): structure F2 is similar to worms but features much thicker walls, whereas structure F3 has locally straight contours paving the available space and sometimes displays regularly spaced lines.

The distinction between worms, spirals and filaments is not always clear. The differences lie in the size of the excrescences and the coiling of their walls; therefore, they could possibly be seen as the same pattern with some scale alterations. However, we preserve this distinction in this work. Note also that the

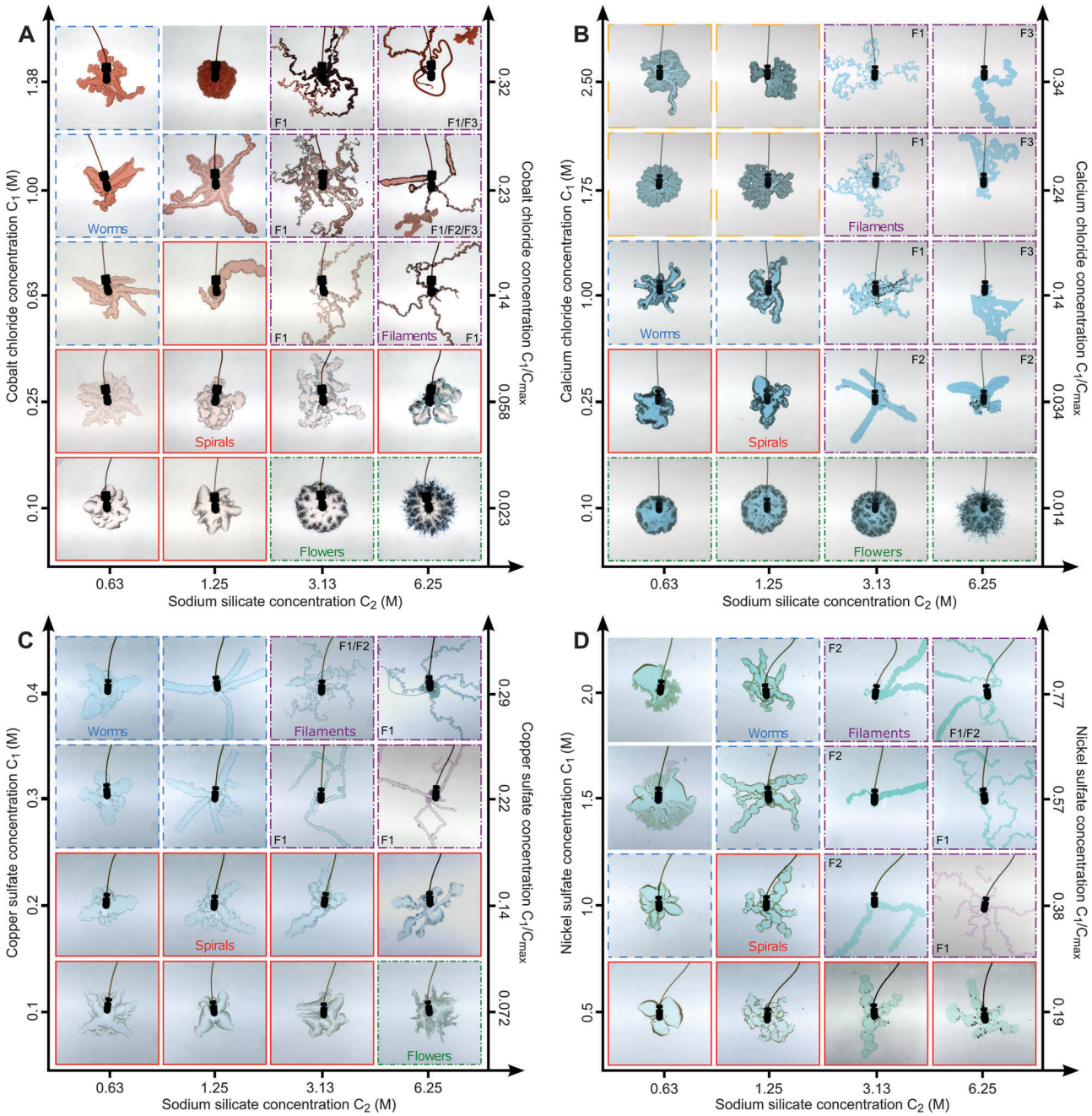

Fig. 2 Phase diagram for $CoCl_2$ (A), $CaCl_2$ with food colouring (B), $CuSO_4$ (C) and $NiSO_4$ (D) injected into sodium silicate. A diagram similar to (A) has been published in ref. 29. The left and right vertical axes show the concentration of the metallic salt solution and this concentration normalized by C_{max}, the limit of solubility for the metallic salt in water, respectively. C_{max} = 4.33 M for $CoCl_2$, 7.32 M for $CaCl_2$, 1.38 M for $CuSO_4$ and 2.61 M for $NiSO_4$.[33] The horizontal axis shows the concentration of sodium silicate. The injection flow rate is 0.11 mL s^{-1} and the field of view is 15 cm × 15 cm. The images are obtained 15 s after the beginning of the injection, which is the typical time needed to obtain well developed macroscopic patterns in the cell.

transition between them when the concentrations or flow rate are varied is typically continuous rather than a transition at a critical value of the parameters.

3 Influence of the metallic salt solution

We first study changes in the precipitation patterns when the metallic salt is varied. We chose the cations calcium, cobalt, copper, and nickel from period 4 of the periodic table, for direct comparison with earlier work in 3D chemical gardens.[22] Patterns obtained by injecting at a constant flow rate calcium chloride, $CaCl_2$, copper sulfate, $CuSO_4$, and nickel sulfate, $NiSO_4$, into a sodium silicate solution are shown in Fig. 2B–D for different concentrations of the metallic salt and silicate solutions at a fixed flow rate. These three phase diagrams together with the reference one for cobalt chloride (Fig. 2A) present similar trends.

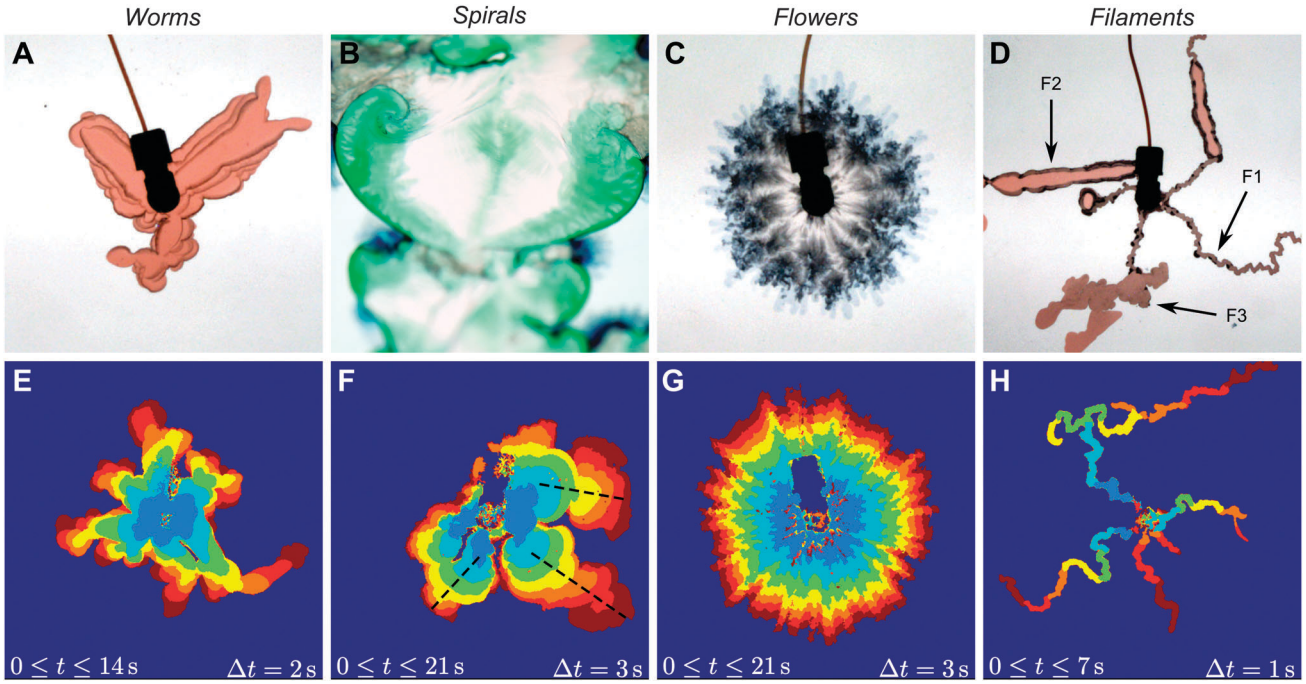

Fig. 3 (A)–(D) Representative images of various pattern regimes shown in Fig. 2A. The field of views are 11.5 cm × 11.5 cm for (A) and (C), 2.5 cm × 2.5 cm for (B) and 15 cm × 15 cm for (D). (D) The image shows three types of structures, termed F1, F2 and F3, which can, as here, sometimes coexist in the same experiment. (E)–(H) Plots showing the evolution in time of similar patterns as in (A)–(D) with a field of view 12 cm × 12 cm. Each colour corresponds to the area added during a time interval Δt as indicated on the panel. Along the black dashed lines of panel (F), the spiral generation process repeats a second time.

In all cases, filaments are observed when both solutions are the most concentrated. Worms emerge when the metallic salt solution is concentrated whereas the alkaline solution is more diluted. Flowers are formed when a low concentration metallic salt solution is injected into the most concentrated sodium silicate solution or for all sodium silicate concentrations when $CaCl_2$ is injected. Spirals are observed for low concentration metal-ion solutions over a large range of concentrations of the alkaline solution. The narrow filaments of type F1 sometimes emerge together with the two other F2 and F3 structures; see Fig. 3D. However, for $CaCl_2$, those structures seem to appear separately depending on the pairs of concentrations (Fig. 2B). Moreover, for the highest concentration of $CaCl_2$ considered in Fig. 2B and for low sodium silicate concentrations, a further type of fingered structure emerges.

These qualitative observations are rationalized in Fig. 4, where a global phase diagram collecting the observed worm, spiral, flower and filament patterns is presented. To compare the different phase diagrams, we note that the limit of solubility in water, C_{max}, of the metallic salt used in the injected solution depends on the nature of the ions. The concentrations of the metallic salt are therefore normalized by C_{max}; see the right vertical axis of the phase diagrams of Fig. 2. This normalization shows that similar patterns are observed in similar regions of the renormalized phase diagram; see Fig. 4. Each type of emerging structure is associated with a given colour and each metallic salt is represented by a given symbol. The coloured areas show the approximate regions where each pattern is generally observed. The fact that similar structures are observed for $CoCl_2$, $CaCl_2$, $CuSO_4$ and $NiSO_4$ in the same regions of the parameter space suggests that the chemical composition of the metallic salt is not the key factor for the pattern selection. We note however that a few small overlaps exist, which may point to the need to incorporate other effects into the renormalization, or perhaps may result from the imprecision in identifying the correct pattern. For example, spirals are sometimes hardly distinguishable from worms; the transition

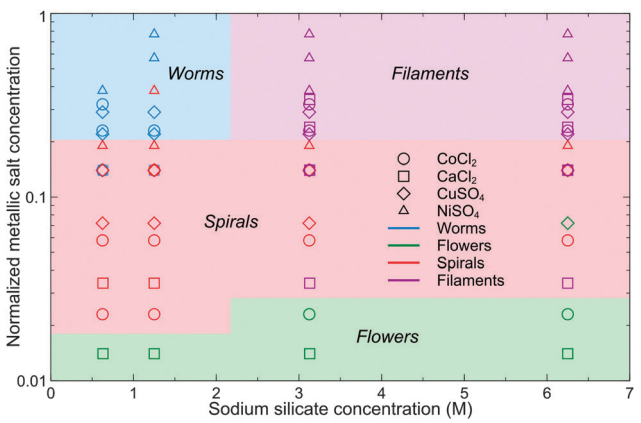

Fig. 4 Phase diagram showing the distribution of the observed patterns for four different metallic salts ($CoCl_2$, $CaCl_2$, $CuSO_4$, $NiSO_4$) injected with the same flow rate into sodium silicate. The vertical axis is the normalized concentration of the metallic salt in a logarithmic scale and the horizontal axis is the concentration of the alkaline solution.

between these two patterns probably being continuous. Additional experiments will be needed to define more accurately the borders of each region of this diagram. Nevertheless, it is already useful to guide future experiments with which this map may be refined.

The formation of chemical gardens takes place in presence of steep pH variations between the metallic salt and the alkaline solution. We have therefore investigated the possible role of the pH of the metallic salt solutions. Table 1 shows that the pH of $CoCl_2$ solutions used in the reference diagram (Fig. 2A) varies by two units within the range of concentrations used. Since the precipitation reaction could be influenced by both the pH and concentration of reactants, we need to disentangle these two effects on the pattern selection. For this purpose, sulfuric acid, H_2SO_4, may be added to the cobalt chloride solution to alter the pH without changing the metallic salt concentration. The resulting patterns are compared in Fig. 5. The first column shows reference patterns obtained when injecting $CoCl_2$ into sodium silicate with various concentrations, whereas the second column shows those resulting from the same experiments when sulfuric acid is added to the $CoCl_2$ solution to lower its pH. In all cases, no significant differences are observed in the precipitation patterns, which suggests that the variation in morphology when the concentration of $CoCl_2$ is varied is not related to the associated change in pH of the metallic salt solution. To check the role of the counter ion, the third column of Fig. 5 shows the structures obtained when solutions of cobalt sulfate, $CoSO_4$, are injected into solutions of sodium silicate at the same concentrations as for $CoCl_2$. Again, in all cases, there are no significant differences between the various precipitation patterns whether the chloride or sulfate is used, which confirms that the non-precipitating counter ion of the metallic salt is not important for the pattern selection.

Finally, we note that the viscosity contrast between the injected and displaced solutions is also not one of the main factors driving the large variety of patterns observed here. Indeed, Table 1 shows that for the three lowest concentrations of sodium silicate used in the reference diagram (Fig. 2A), the viscosity ratio between the injected metallic salt solution and the displaced alkaline solution is essentially constant and close to 1. Therefore, a hydrodynamic viscous fingering instability[30,31,34,35] cannot account for the various patterns observed in this region of the diagram. For the largest silicate concentration of 6.25 M, the displaced silicate solution is roughly 35 times more viscous than the injected cobalt one, which could lead to viscous fingering. We also note, however, that, when the cobalt chloride concentration is increased from 0.1 M to 0.25 M, the viscosity contrast remains the same while the pattern evolves from flowers to spirals (Fig. 2A). Such a change in morphology cannot be explained by viscous effects.

Viscous fingering can account for the formation of flowers at the lowest cobalt concentration. Indeed, as seen in Fig. 3C, blue viscous fingers grow ahead of the dark precipitate, which is less cohesive and is carried along with the flow. However, as the concentration of metallic salt increases, the precipitate is more cohesive and forms a barrier between the two fluids. The breaking of this wall and its rotation around the breaking point has been shown to lead to the growth of logarithmic spirals.[29] The growth dynamics of the spirals is therefore quite different from that of the flowers and is independent from viscosity contrasts. This is reminiscent of the observation made in classical

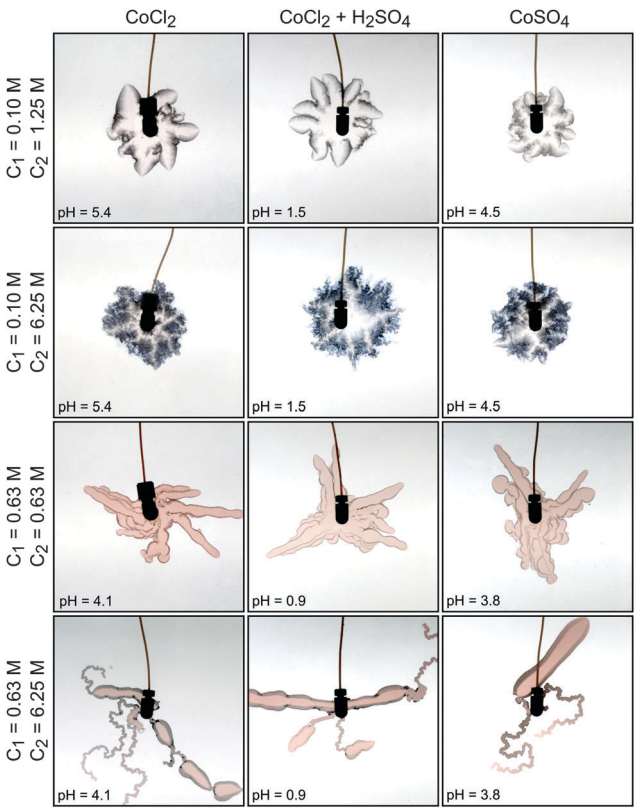

Fig. 5 Influence of the pH and the metallic salt anion on the pattern selection. Solutions of $CoCl_2$, $CoCl_2$ with sulfuric acid and $CoSO_4$ at a concentration C_1 are injected into solutions of sodium silicate at a concentration C_2. The pH of the metallic salt solutions is indicated. The constant injection flow rate is 0.11 mL s^{-1} and the field of view is 15 cm × 15 cm. The images are obtained 15 s after the beginning of the injection.

Table 1 Density ρ, pH and viscosity μ of cobalt chloride, sodium silicate and sodium carbonate solutions as a function of their concentration

	ρ (g cm^{-3})	pH	μ (mPa s)
[$CoCl_2$] (M)			
0.10	1.01	5.4	1.1
0.25	1.03	4.6	1.2
0.63	1.07	4.1	1.4
1.00	1.11	3.7	1.6
1.38	1.15	3.4	1.7
[Sodium silicate] (M)			
0.63	1.04	11.6	1.3
1.25	1.09	11.7	1.7
3.13	1.21	11.7	3.6
6.25	1.42	11.8	~40
[Na_2CO_3] (M)			
0.25	1.02	11.4	1.2
0.63	1.03	11.5	1.4
1.25	1.12	11.6	2.0
2.50	1.23	11.6	4.4

chemical gardens in 3D (*i.e.*, without injection) that solid tubes are formed only if the salt concentration is large enough.[1,2] Here, similarly, the pattern is influenced by viscous effects at the largest silicate concentration if the salt concentration is low and the precipitate not cohesive enough. A switch to other patterns like spirals and filaments is obtained when the resistance to flow of the more cohesive solid precipitate is larger as the salt concentration increases at fixed silicate content.

4 Influence of the alkaline solution

Having established the genericity of the quasi-2D precipitate patterns with respect to varying the nature of the metallic salt, we now focus our attention on the influence of the changes in the nature of the alkaline reactant. For this purpose, cobalt chloride is maintained as the metallic salt to allow direct comparison with the reference phase diagram shown in Fig. 2A, while sodium silicate is replaced by sodium carbonate, Na_2CO_3. Table 1 shows that the density, the pH and the viscosity are similar for both solutions of sodium silicate and sodium carbonate. The resulting phase diagram is shown in Fig. 6. Again, we observe similar morphologies for the precipitation patterns. Filaments are still obtained when both solutions are concentrated, flowers emerge when the solution of $CoCl_2$ is dilute, whereas worms are selected when the metallic solution is concentrated and the alkaline solution is dilute. But even though the global trends of the reference diagram are recovered when sodium carbonate is used instead of sodium silicate, there do exist some differences. First a new "star" pattern is observed when both reactants are at 0.25 M concentration, in which a eight-branched star pattern of liquid $CoCl_2$ remains imprinted at the rear of the outer circular rim of precipitate in the early injection process. And from a quantitative point of view, we notice in Fig. 6 the presence of flower patterns for concentrations of $CoCl_2$ of 0.25 M for carbonate whereas for such a concentration of metallic salt, spiral patterns emerge for silicate (Fig. 2A). This difference highlights, as previously discussed, that the boundaries of the regions of the phase diagram shown in Fig. 4 are not sharp.

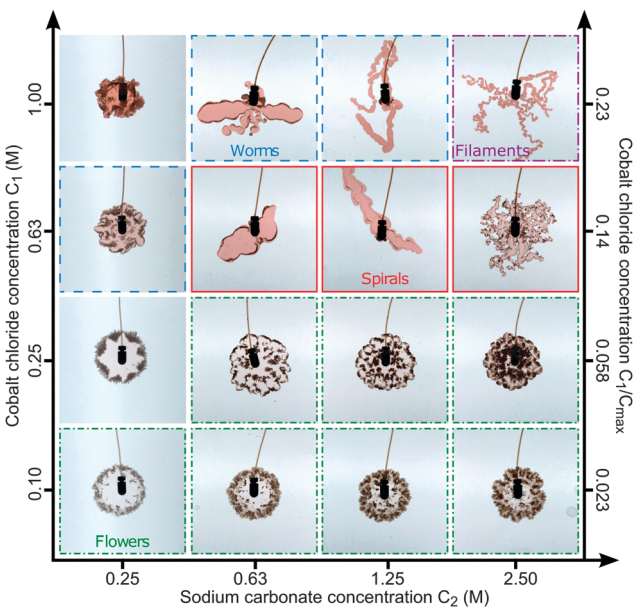

Fig. 6 Phase diagram for $CoCl_2$ injected into Na_2CO_3. The injection flow rate is 0.11 mL s^{-1} and the field of view is 15 cm × 15 cm. The images are obtained 15 s after the beginning of the injection.

This slight shift of boundaries between different types of patterns when the alkaline reactant is changed may be due to the fact that, when reacting with carbonate, a larger concentration of metallic salt is required to obtain a sufficiently cohesive precipitate to form the solid barrier needed to produce spiral patterns; see the model in ref. 29. This observation implies that simply rescaling the concentration of the metallic salt by C_{max} is not sufficient to produce a universal phase diagram; an additional rescaling taking into account the mechanical properties of the precipitate should also be considered to refine the comparison.

5 Discussions and conclusions

We have here experimentally compared chemical gardens grown in a confined geometry when cobalt, calcium, nickel and copper salt solutions are injected radially into an alkaline solution of either silicate or carbonate initially filling a horizontal Hele-Shaw cell. We have shown that the general trends of the phase diagrams of the precipitate structures obtained upon changes of concentrations at a fixed flow rate are robust to changes in the nature of the reactant ions. Indeed, the morphologies of the patterns emerging in given concentration regimes are not significantly sensitive to changes in the chemical nature of the reactive ions. Both the precipitating cation and the non-precipitating anion of the metallic salt have been changed, while silicate has also been replaced by carbonate, without major influence on the main resulting structures. The global trends for the pattern selection as a function of the concentrations of both injected and displaced solutions are preserved. All patterns obtained with silicate can be reasonably gathered in a general phase diagram in which the concentration of the metal salt is renormalized by its solubility in water. A slight shift of the zones is observed when silicate is replaced by carbonate, suggesting that the cohesive properties of the precipitate might also be important in the definition of a universal phase diagram.

Our results thus support the hypothesis that the specific identities of the ions involved are not crucial to explain the pattern selection in confined chemical gardens. The focus should thus be put on physical phenomena to understand and model this selection and to forge a link between chemical garden precipitates and other patterns obtained in similar growth conditions with other reactions.[30–32] For example, the relative viscosity and density of the two solutions may control the observed structures in some regions of the phase diagram (flower pattern for instance). The cohesive strength of the agglomerate of precipitate, measured as the force per unit area it can sustain before rupture, compared to the fluid pressure should also be an important parameter to understand the various morphologies observed in our experiments.

The time needed to form a cohesive agglomerate of precipitate, which varies with the concentrations, compared to the hydrodynamic time, controlled by the injection rate, is certainly also an important factor influencing the overall pattern selection. Indeed, as soon as the two fluids are in contact, a fast precipitation reaction occurs at the contact zone and forms a thin porous layer. The time scale associated with this precipitation process is related to the chemical reaction time scale, T_{chem}, which is very small since the precipitation reaction is very fast. However, as soon as this porous layer is formed, further precipitation leading to the hardening of the structure is only possible if the ions diffuse through the already formed porous layer. This hardening time, T_{hard}, is given by the time needed for ions to diffuse through a porous medium of thickness $h(t)$, which increases with time. This time scale is thus expected to be much longer than T_{chem} since it involves diffusion through a porous phase. The interplay between these time scales should be another factor influencing the pattern selection.

Finally, notice that we have here studied only the patterns developing during the first few seconds after the beginning of injection. On longer time scales, other growth mechanisms influenced by diffusion take place. Further precipitation structures that depend on the reactants used appear.[29] The understanding of these later-stage evolutions of the precipitate structures certainly relies on chemical specificities of the products formed and hence on the chemical reactants involved. At sufficiently low injection rate such that diffusion dominates over advection, the specific nature of the ions should also be an important factor to explain the patterns. These phenomena still demand further analysis, which we intend to accomplish in future investigations.

6 Materials and methods

Solutions—The different metallic salt solutions are prepared by the dissolution in distilled water of cobalt chloride hexahydrate, nickel sulfate hexahydrate, copper sulfate pentahydrate and calcium chloride dihydrate (Sigma Aldrich). The sodium silicate solutions are obtained by dilution of a commercial solution of concentration 6.25 M with respect to silica (Sigma Aldrich), whereas the carbonate solutions are obtained by dissolution of a sodium carbonate powder in water (Sigma Aldrich). The pH of the solutions is measured with a pH-meter (Radiometer Analytical Ion Check 10) at a fixed temperature of 20 °C. The viscosities are measured with a Brookfield LVDV II Pro. The densities are measured with a DMA Anton Paar densimeter. Hele-Shaw set up—The experimental set up (Fig. 1) is a horizontal Hele-Shaw cell composed of two acrylate plates (205 mm × 205 mm × 8 mm) separated by a small gap (0.5 mm) with a plastic spacer. The cell is filled initially with the alkaline reactant (silicate or carbonate solution). The metallic salt is injected radially through a hole in the lower plate. The injection device comprises a syringe pump and a capillary tube, linked from one side to the syringe *via* a Luer lock connector. From the other side, a connector links the tube to the cell with no contact between the two fluids before injection starts at a controlled given flow rate imposed by the syringe pump. The set-up is illuminated from below by a light pad and the dynamics is recorded from above using a camera (either an Allied or a Pixelink digital camera).

Acknowledgements

We thank E. Schmitz for help with the pH measurements. A.D., F.B. and F.H. acknowledge PRODEX and FRS-FNRS (FORECAST project) for financial support. J.H.E.C. acknowledges the financial support of MICINN grant FIS2013-48444-C2-2-P.

References

1 R. D. Coatman, N. L. Thomas and D. D. Double, *J. Mater. Sci.*, 1980, **15**, 2017–2026.
2 J. H. E. Cartwright, J. M. García-Ruiz, M. L. Novella and F. Otálora, *J. Colloid Interface Sci.*, 2002, **256**, 351–359.
3 T. Hazlehurst, *J. Chem. Educ.*, 1941, **18**, 286–289.
4 W. Duan, S. Kitamura, I. Uechi, A. Katsuki and Y. Tanimoto, *J. Phys. Chem. B*, 2005, **109**, 13445–13450.
5 F. Glaab, M. Kellermeier, W. Kunz, E. Morallon and J. M. Garcia-Ruiz, *Angew. Chem.*, 2012, **51**, 4317–4321.
6 G. Butler and H. C. K. Ison, *Nature*, 1958, **182**, 1229–1230.
7 D. D. Double and A. Hellawell, *Nature*, 1976, **261**, 486–488.
8 J. H. E. Cartwright, B. Escribano, D. L. Gonzalez, C. I. Sainz-Díaz and I. Tuval, *Langmuir*, 2013, **29**, 7655–7660.
9 J. B. Corliss, J. Dymond, L. I. Gordon, J. M. Edmond, R. P. von Herzen, R. D. Ballard, K. Green, D. Williams, A. Bainbridge, K. Crane and T. H. van Andel, *Science*, 1979, **203**, 1073–1083.
10 G. J. T. Cooper, A. G. Boulay, P. J. Kitson, C. Ritchie, C. J. Richmond, J. Thiel, D. Gabb, R. Eadie, D.-L. Long and L. Cronin, *J. Am. Chem. Soc.*, 2011, **133**, 5947–5954.
11 S. Thouvenel-Romans and O. Steinbock, *J. Am. Chem. Soc.*, 2003, **125**, 4338–4341.
12 J. Maselko, P. Borisova, M. Carnahan, E. Dreyer, R. Devon, M. Schmoll and D. Douthat, *J. Mater. Sci. Lett.*, 2005, **40**, 4671–4673.
13 J. J. Pagano, T. Bánsági, Jr. and O. Steinbock, *Angew. Chem., Int. Ed.*, 2008, **47**, 9900–9903.
14 R. Makki, M. Al-Humiari, S. Dutta and O. Steinbock, *Angew. Chem., Int. Ed.*, 2009, **48**, 8752–8756.
15 R. Makki, L. Roszol, J. J. Pagano and O. Steinbock, *Philos. Trans. R. Soc., A*, 2012, **370**, 2848–2865.
16 R. Makki and O. Steinbock, *J. Am. Chem. Soc.*, 2012, **134**, 15519–15527.
17 L. Roszol, R. Makki and O. Steinbock, *Chem. Commun.*, 2013, **49**, 5736–5738.
18 R. Makki, X. Ji, H. Mattoussi and O. Steinbock, *J. Am. Chem. Soc.*, 2014, **136**, 6463–6469.
19 L. M. Barge, I. J. Doloboff, M. J. Russell, D. VanderVelde, L. M. White, G. D. Stucky, M. M. Baum, J. Zeytounian, R. Kidd and I. Kanik, *Geochim. Cosmochim. Acta*, 2014, **128**, 1–12.
20 M. J. Russell and A. Hall, *J. Geol. Soc.*, 1997, **154**, 377–402.

21 L. M. Barge, I. J. Doloboff, L. M. White, G. D. Stucky, M. J. Russell and I. Kanik, *Langmuir*, 2012, **28**, 3714–3721.
22 J. H. E. Cartwright, B. Escribano and C. I. Sainz-Díaz, *Langmuir*, 2011, **27**, 3286–3293.
23 J. H. E. Cartwright, B. Escribano, S. Khokhlov and C. I. Sainz-Díaz, *Phys. Chem. Chem. Phys.*, 2011, **13**, 1030–1036.
24 A. Tóth, D. Horváth, R. Smith, J. R. McMahan and J. Maselko, *J. Phys. Chem. C*, 2007, **111**, 14762–14767.
25 S. Thouvenel-Romans and O. Steinbock, *J. Am. Chem. Soc.*, 2003, **125**, 4338–4341.
26 S. Thouvenel-Romans, W. van Saarloos and O. Steinbock, *Europhys. Lett.*, 2004, **67**, 42–48.
27 R. Clément and S. Douady, *Europhys. Lett.*, 2010, **89**, 44004.
28 S. Thouvenel-Romans, J. J. Pagano and O. Steinbock, *Phys. Chem. Chem. Phys.*, 2005, **7**, 2610–2615.
29 F. Haudin, J. H. E. Cartwright, F. Brau and A. De Wit, *Proc. Natl. Acad. Sci. U. S. A.*, 2014, **111**, 17363–17367.
30 T. Podgorski, M. C. Sostarecz, S. Zorman and A. Belmonte, *Phys. Rev. E: Stat., Nonlinear, Soft Matter Phys.*, 2007, **76**, 016202.
31 Y. Nagatsu, S.-K. Bae, Y. Kato and Y. Tada, *Phys. Rev. E: Stat., Nonlinear, Soft Matter Phys.*, 2008, **77**, 067302.
32 Y. Nagatsu, Y. Ishii, Y. Tada and A. De Wit, *Phys. Rev. Lett.*, 2014, **113**, 024502.
33 *CRC Handbook of Chemistry and Physics*, ed. D. R. Lide and W. M. Haynes, CRC Press, Boca Raton, Florida, 90th edn, 2010.
34 S. H. Hejazi, P. M. J. Trevelyan, J. Azaiez and A. De Wit, *J. Fluid Mech.*, 2010, **652**, 501–528.
35 L. A. Riolfo, Y. Nagatsu, S. Iwata, R. Maes, P. M. J. Trevelyan and A. De Wit, *Phys. Rev. E: Stat., Nonlinear, Soft Matter Phys.*, 2012, **85**, 015304(R).